Journal of Applied Fluid Mechanics, Vol. 17, No. 2, pp. 410-423, 2024.
Available online at www.jafmonline.net, ISSN 1735-3572, EISSN 1735-3645.
https://doi.org/10.47176/jafm.17.02.2101

Analysis of Flow Field Distortion in Ship Inlet System and Its Effect on Compressor Performance

Z. Y. Wang, C. X. He† and Y. L. Qu

Harbin Engineering University, Nantong Street 145. Harbin, Heilongjiang Province, 150001, China

†*Corresponding Author Email: 821901156@hrbeu.edu.cn*

ABSTRACT

Intake system structure design is categorized under gas turbine marine technology, and its performance affects the inlet flow field of the compressor, thereby impacting the overall operation stability of the gas turbine. Therefore, this study analyses the structural characteristics of various types of intake systems and establishes a computational domain model. Numerical simulation methods are used to systematically study the internal and external flow fields of the intake system. By varying the structure of the intake system, we compare and study the distribution form of the flow field inside and outside the intake system, velocity and total pressure distribution of the compressor inlet section, and flow loss inside the intake system. The speed and total pressure distortion of the compressor inlet section are analysed quantitatively. It was concluded that inlet distortion causes the leakage flow from some channels to spill into adjacent blade channels at the leading edge of the higher span, resulting in an early compressor stall. Specifically, the compressor stall and working flow margins are reduced by 2.51% and 2.76%, respectively.

Article History

Received June 18, 2023
Revised August 11, 2023
Accepted October 3, 2023
Available online December 4, 2023

Keywords:

Ship intake structure
Inlet distortion
Structural modification
Axial compressor
Compressor performance

1. INTRODUCTION

Over the past 70 years, gas turbines have undergone various stages of research and development, testing, trial use, and actual ship operations, to become one of the primary power sources for contemporary ships (Soemarwoto et al., 2016). Currently, gas turbines are extensively used in large surface ships and small high-performance ships such as air cushion landing crafts, hydrofoil boats, military transport ships, ice breakers, and civilian ships (Chen et al., 2016). The design of an intake system is critical in the installation of gas turbines on various types of ships, and the intake design directly affects the overall performance, reliability, and service life of gas turbines. The operation of the gas turbine of a ship requires a large intake flow rate (Bricknell, 2006). Inlet distortion caused by uneven airflow in the intake flow field can result in a decrease in compressor efficiency and surge margin, affecting the stability of gas turbine operation. Therefore, the uniformity of the flow field in the compressor inlet section is crucial for the optimal performance of marine gas turbine inlet systems (Wang et al., 2017).

The inlet flow field of the gas turbines of a ship requires high uniformity and low pressure loss. However, limited space resources on ships restrict the shapes and sizes of the gas turbine intake systems. The airflow typically needs to be rotated 90° in front of the compressor, resulting in uneven intake. Therefore, this study aims to design various intake structures within the limited intake space available in a ship and simulate the flow field characteristics of the gas turbine intake system. Furthermore, we analysed the influence of different intake structures and distortions of the ship on the characteristics of the intake flow field and the studied compressor, respectively.

To understand the influence of the intake structures of marine gas turbines on the flow field of the intake system, researchers (Sutherland, 2008; Winter, 2009; Xu et al., 2014) used the velocity uniformity of the compressor inlet to analyse the impact of various intake structures on the flow field. The analyses were performed by varying the structural parameters such as intake area, intake angle, and airflow direction. Wen & Xiao (2010) analysed the flow field changes in an intake system under different operating conditions based on the non-uniformity of the total pressure. Simultaneously, significant research have been devoted to analysing the impact of inlet distortion on compressors and guiding their anti-distortion design. Since 1950, researchers have conducted a series of experiments to investigate the impact of inlet distortions on compressor performance (Cossar et al. 1980; Fuqun et al. 1985; Hynes & Greitzer, 1987). They preliminarily concluded that distortion can lead to premature instability of the compressor and even surge. Subsequent research has revealed that distortion exacerbates the occurrence of stall units. Additionally, the influence of the distortion velocity and stall unit propagation speed on the stability

NOMENCLATURE

D_1	distance between the top edge of the baffle and the bottom corner	**Greek Letters**	
D_2	distance between the lower edge of the baffle and the bottom corner	δ	compressor inlet velocity distortion
DP_1	compressor inlet pressure distortion 1	Ω_S	compressor stall margin
DP_2	compressor inlet pressure distortion 2	Ω_m	compressor working flow margin
A_i	grid node area	π	pressure ratio
$\overline{P}$	average pressure of cross-section	**Abbreviation**	
m	mass flow rate	SS	small ship model
X	flow direction position	SM	small ship modification model
$\overline{V}_A$	average velocity of cross-section	PE	highest efficiency operating point
$\overline{V}_{\min}$	average velocity in high-speed areas	NS	near stall operating point
$\overline{V}_{\max}$	average velocity in high-speed areas	D	compressor blade passage

was more pronounced. Despite these critical findings, distortion testing poses significant challenges owing to its high cost and associated risks; therefore, computational fluid dynamics (CFD) calculations have become another option for distortion testing. By analysing the influence of distortion on aerodynamic loss, researchers have conducted numerical simulations (Hah et al., 1996; Hirai et al., 1997; Charalambous et al., 2004; Yao et al., 2010; Fidalgo et al., 2012; Zhao et al., 2017; Dong et al., 2018; Sun et al., 2018; Li et al., 2020; Jahani et al., 2022). These simulations have demonstrated that the interaction between the impact and blade boundary layer is enhanced under distortion conditions, leading to an increase in aerodynamic loss and a reduction in the stall margin. Zhang and Zheng (2017) proposed a method to determine the optimal match between the inlet and outlet distortions to improve the performance of centrifugal compressors.

In the above studies, when analysing the uniformity of ship intake, single velocity or pressure parameters were used to study the uniformity of the flow field, and a single-intake structure was used for the analysis. This study focuses on investigating the representative inlet structures of ships. Specifically, various ship inlet structures were evaluated by changing the angle of the inlet shaft, modifying the volume of the pressure-stabilising chamber, and installing baffles and decelerators. The uniformity of the compressor inlet was quantitatively analysed using velocity distortion and total pressure distortion parameters. The flow state of each intake structure was determined through numerical simulations, facilitating the analysis of the effects of ship inlet distortion on the flow rate, efficiency, and stall margin of the compressor. Finally, this research provides valuable guidance for ship intake system and anti-distortion compressor designs.

2. PHYSICAL MODEL OF SHIP INTAKE AND EXHAUST SYSTEMS

2.1 Establishment of Calculation Model

This study investigated the intake system of a marine gas turbine and conducted a comprehensive analysis of the selected intake system and structure of an actual ship, based on drawings of the ship. The characteristics and dimensions of each part were then carefully determined, and a three-dimensional model of the entire ship and related computational domain was constructed using a modelling software. This large ship model encompassed various components, including the intake compartment, intake shutter, shaft, silencer, intake filter compartment, pressure-stabilising chamber, communication channel, box body, gas turbine, exhaust ejector, exhaust volute, intake volute, and parts of the hull. The overall three-dimensional model of the large ship and external environmental space was a rectangular body measuring 14000 mm × 10000 mm × 5000 mm (Fig. 1(a)). The small-ship model included an intake shutter, a pressure-stabilising chamber, a compressor inlet, and a reducer installed within the stabiliser box, as shown in Fig. 1 (c). The dimensions of the small ship model were 3300 mm × 3100 mm × 2400 mm.

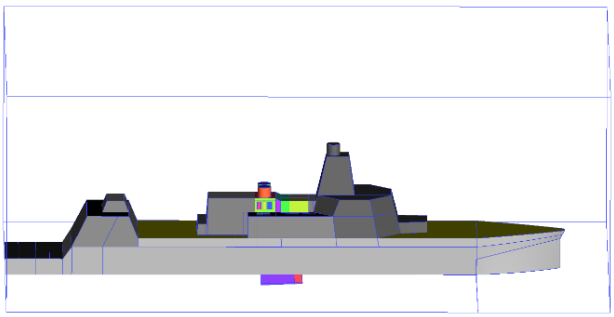

(a) Large ship model

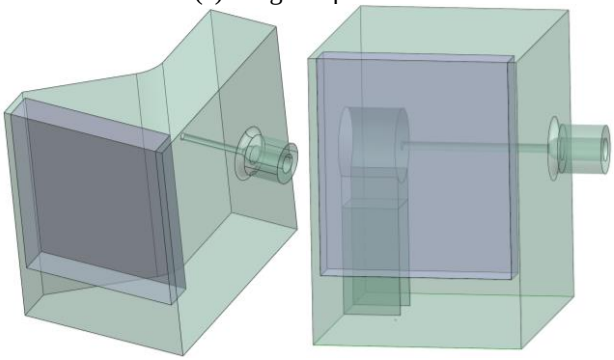

(b) Small ship model (c) Small ship modification model

Fig. 1 Overall ship model

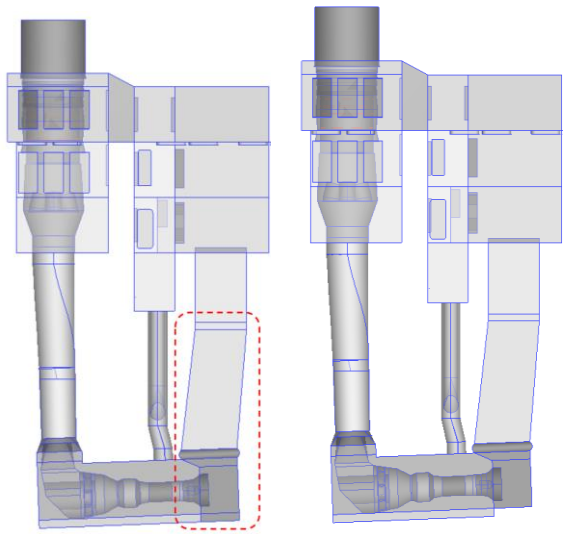

(a) Original model (b) Plan I

(c) Plan II (d) Plan III

Fig. 2 Different intake system structure

In this study, modifications were made to the original model by altering the intake system structure. The surge chamber and intake shaft were identified as having the greatest impact on the unevenness of the compressor inlet flow field and were targeted for structural changes. Three different plans were developed: Plan I reduced the volume of the intake pressure stabilizing chamber, to decrease air flow space. Plan II altered the vertical angle of the intake shaft. Plan III introduced a baffle in the intake pressure stabilizing chamber, altering the flow mode of the airflow in the surge chamber by tweaking the baffle parameters. These modifications were made to assess the impact of different intake system structures on the uniformity of compressor inlet flow.

In this study, we investigated the influence of baffle parameters on the compressor inlet flow field by comparing the numerical simulation results obtained from four different baffle forms installed in the stabilising chamber of Plan III. The specific parameters of each baffle are listed in Table 1. D_1 and D_2 shown in Fig. 3, represent the distance between the edge of the baffle and bottom corner of the pressure-stabilising chamber.

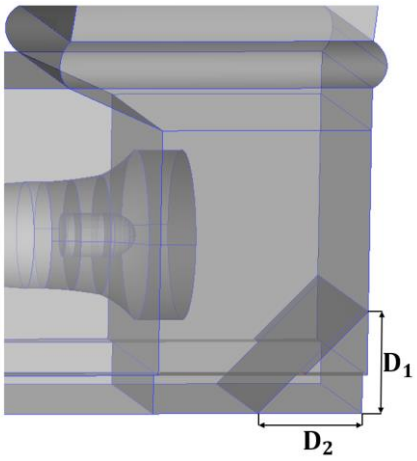

Fig. 3 Plan III different types of baffles

Table 1 Plan III baffle parameters

Baffle parameters	Plan IIIa	Plan IIIb	Plan IIIc	Plan IIId
D_1 **(mm)**	900	1350	900	1350
D_2 **(mm)**	900	900	1350	1350

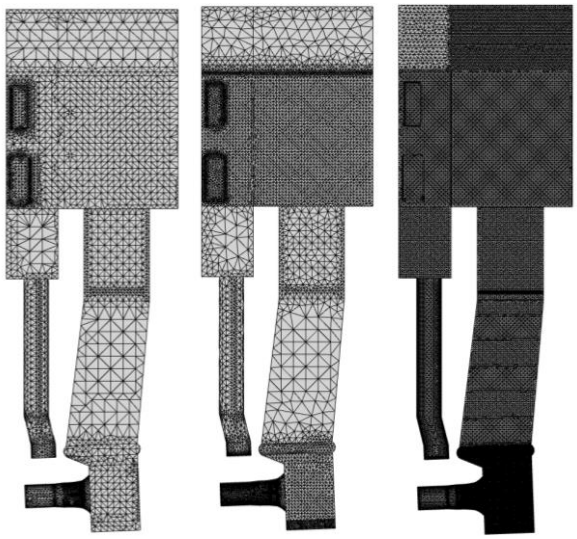

(a)Grid 1 (b)Grid 2 (c)Grid 3

Fig. 4 Grid division scheme

2.2 Meshing

For large air intake systems, the computational domain model and complex structure require the use of an unstructured grid division that employs a grid division tool to accurately reflect the internal flow field characteristics. The boundary of the calculation domain for each component was set as the interior, and a boundary layer was added to the complex flow in the inlet section of the compressor. The height of the first-layer grid was 0.5 mm, minimum orthogonality greater than 18, and the unit growth rate was 1.2. To verify the independence of grid partitioning, we performed grid encryption based on the proposed grid partitioning scheme. The calculation model adopts three grid division scales: Grid 2 mainly encrypts components with significant flow changes in the intake

Table 2 Grid independence verification

	Grid 1	Grid 2	Grid 3
Investigate parameters	1.78×10^7	1.89×10^7	2.30×10^7
ΔP_{IC} (Pa)	1740.5	1744.1	1745.1

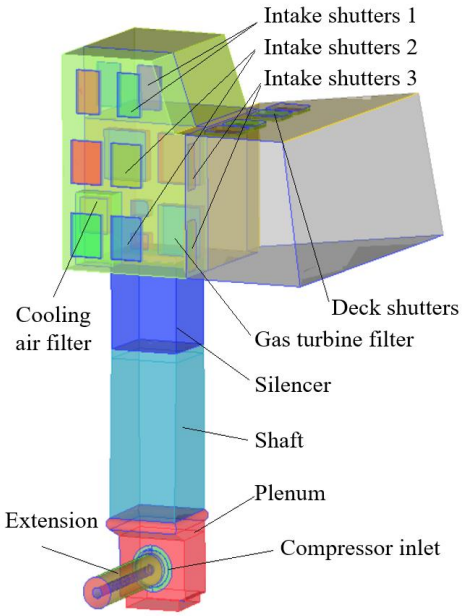

Fig. 5 Geometry of a large ship intake system

chamber, pressure-stabilising chamber, and compressor intake section, whereas Grid 3 further encrypts all the intake components, resulting in a total grid count of 17.8, 18.9, and 23 million grids for the respective scales. A comparison of the key section parameters revealed that they remained mostly unchanged when the number of grids listed in Table 2 exceeded 18.9 million. Therefore, we selected the 18.9 million grid division scheme based on the calculation time. The air intake structure model and grid distribution are shown in Figs 5 and 6, respectively.

3. NUMERICAL SIMULATION SCHEME

3.1 Calculation Scheme and Boundary Conditions

Considering the presence of various complex flow states, such as incompressible, compressible, and high temperatures, within the computational domain and adaptability of the mesh generation software ICEM, ANSYS Fluent software was selected for the simulation calculation of the inlet system of the ship. Owing to the substantial size of the model, it is challenging to ensure that the y^+ values of each component meet the requirements of turbulence models, such as $k-\omega$. To ensure calculation accuracy, the $k-\varepsilon$ two-equation turbulence model was used to solve the Reynolds-averaged Navier–Stokes equations. The marine environment calculation domain was set with an inlet boundary temperature of 300 K and a total pressure of 101325 Pa. The compressor inlet was set as the outlet boundary with a target flow rate of 80 kg/s. The turbine

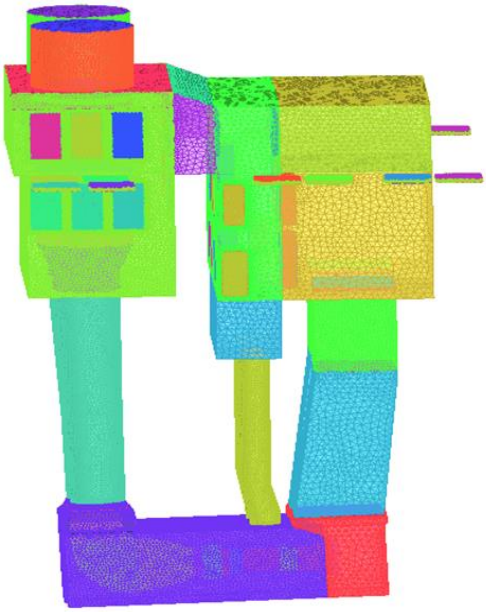

Fig. 6 Large ship intake and exhaust system grid

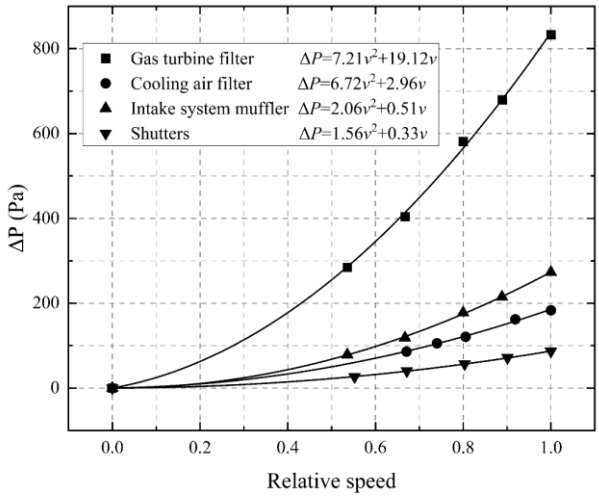

Fig. 7 Porous jump parameters of intake and exhaust component

outlet was set as the mass-flow inlet boundary with a gas temperature and mass flow rate of 753 K and 80 kg/s, respectively. Owing to the overly complex internal structures of the shutters, filters, and silencers, accurate pressure and flow changes were obtained by providing boundary conditions for the porous areas in the Fluent software. The velocity vector in the porous medium was set according to the flow direction, and the permeability of the medium α and pressure step coefficient C_2 of each component were determined according to the relationship between the flow rate of each component and total pressure loss obtained from Equation 1 and the experiment in Fig. 7. Additionally, the porosity was set to 1.

The pressure change in porous media is defined as a combination of the Darcy's law and additional inertia loss term. The parameters for setting the boundary conditions of the porous media were obtained by solving Equation 1.

$$\Delta P = -(\frac{\mu}{\alpha} v + C_2 \frac{1}{2} \rho v^2)\Delta m \tag{1}$$

In the formula, α is the permeability of the medium, C_2 is the pressure step coefficient, v is the normal velocity on the surface of the medium, and Δm is the thickness of the medium.

3.2 Distortion Assessment Method

To evaluate the degree of distortion of the flow field in the compressor inlet flow section, two nondimensional parameters were selected for quantitative analysis, namely velocity and total pressure distortion. Velocity distortion is defined as the ratio of the difference between the local and average velocities of the flow in that section to the average velocity of the flow, as shown in Equation (2).

$$\delta = \frac{\sum |\delta_i| A_i}{\sum A_i} \tag{2}$$

Here, δ_i represents the non-uniformity of each unit over the full section with respect to the mean flow rate, and A_i represents the area of each unit.

The total pressure distortion DP_1 is given by the Equation (3).

$$DP_1 = \frac{\overline{P} - P_{i(60)_{\min}}}{\overline{P}} \times 100\%, \tag{3}$$

Where, $\bar{P}$ is the mean total pressure of the compressor inlet section, and $P_{i(60)}$ is the mean total pressure of the section at 60°.

The total pressure distortion DP_2, was obtained as the ratio of the difference between the mean total pressure and mean total pressure of the low-pressure area surface to the mean total pressure.

$$DP_2 = \frac{\overline{P} - P_{\min}}{\overline{P}} \times 100\% \tag{4}$$

Here, $\bar{P}_{min}$ is below the mean total pressure in the area of the mean total pressure of the face.

The changes in the compressor performance were analysed using the margin definitions of Equations (5) and (6).

$$\Omega_S = \frac{m_{PE}}{m_{NS}} \cdot \frac{\pi_{NS}}{\pi_{PE}} - 1 \tag{5}$$

$$\Omega_M = \frac{m_{BS1} - m_{NS1}}{m_{BS2} - m_{NS2}} \cdot \frac{m_{PE2}}{m_{PE1}} - 1 \tag{6}$$

3.3 Experimental Verification of Numerical Simulation Method

To validate the numerical simulation scheme, it was compared with the small-ship intake system test conducted by Shi et al. (2004). The parameters of the compressor inlet flow section were compared for two models: the test result with a section of X=996 mm and the numerical simulation result with a section of X=2490 mm. These parameters are listed in Table 3, where $\bar{V}_A$ denotes the area-weighted average speed, and $\bar{V}_{max}$ and $\bar{V}_{min}$ represent the area-weighted average speeds above and below the area of $\bar{V}_A$, respectively. The calculated and experimental values were compared based on the above definitions. As shown in Fig. 8, the difference between the velocities of each measurement point along the circumferential direction of the AIP section and corresponding regional velocities of the numerical simulation results was less than 2%. Thus, the simulation scheme used in this study is suitable for subsequent analyses and calculations. The simulation results were sufficiently accurate for exploring the flow in the ship intake systems.

Table 3 Verification of numerical simulations

Investigate parameters	$\bar{V}_A$ (m/s)	$\bar{V}_{max}$ (m/s)	$\bar{V}_{min}$ (m/s)	δ(%)
Experimental results	151.8	154.5	148.9	3.67
Calculation results	151.6	154.8	148.23	3.91

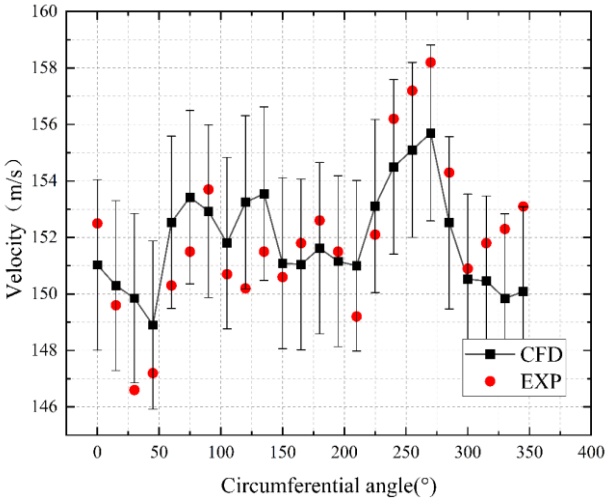

Fig. 8 Verification of simulation results

4. INFLUENCE OF THE INTAKE STRUCTURE OF SHIPS

A comparative analysis of the overall total pressure and velocity distribution using the cloud diagrams of the intake and exhaust systems is shown in Fig. 9. The airflow from the shutters to the outlet of the intake shaft had sufficient flow space, with a small change in the overall velocity and total pressure. The airflow in the pressure-stabilising chamber was affected by the suction effect of the compressor, leading to an evident speed gradient near the cowling. The flow transition from the intake shaft to the compressor was approximately 90°. This flow transition was influenced by structural asymmetries in the pressure stabilizing chamber, resulting in asymmetries in the flow field in the cowl. Despite the fairing serving to rectify the airflow, it was unable to fully eliminate the non-uniformity of the flow, ultimately leading to the distortion of the flow field at the compressor inlet. The overall flow

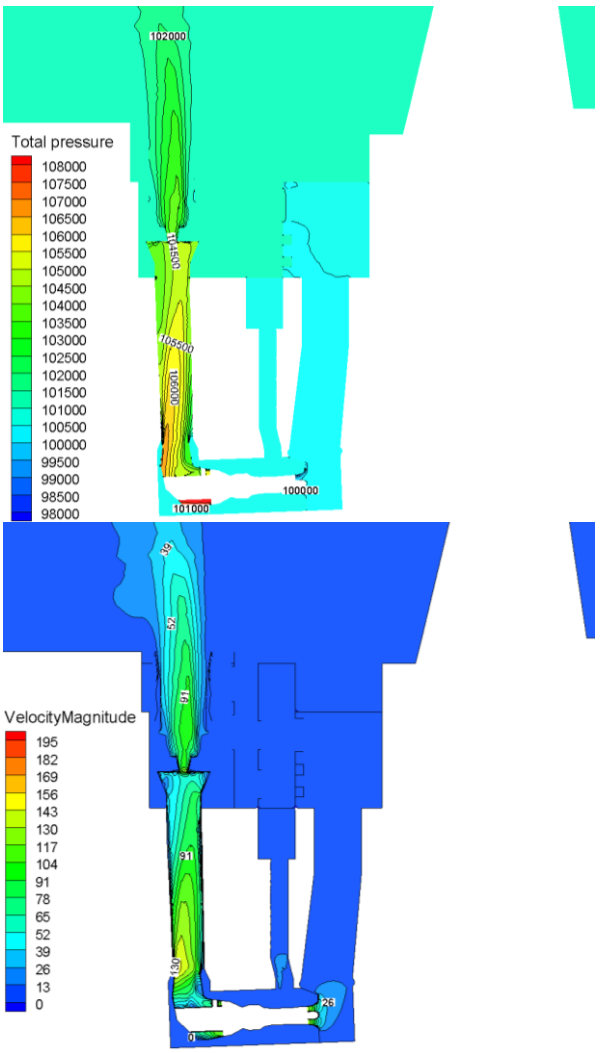

Fig. 9 Total pressure and velocity distribution at large ship intake and exhaust structures

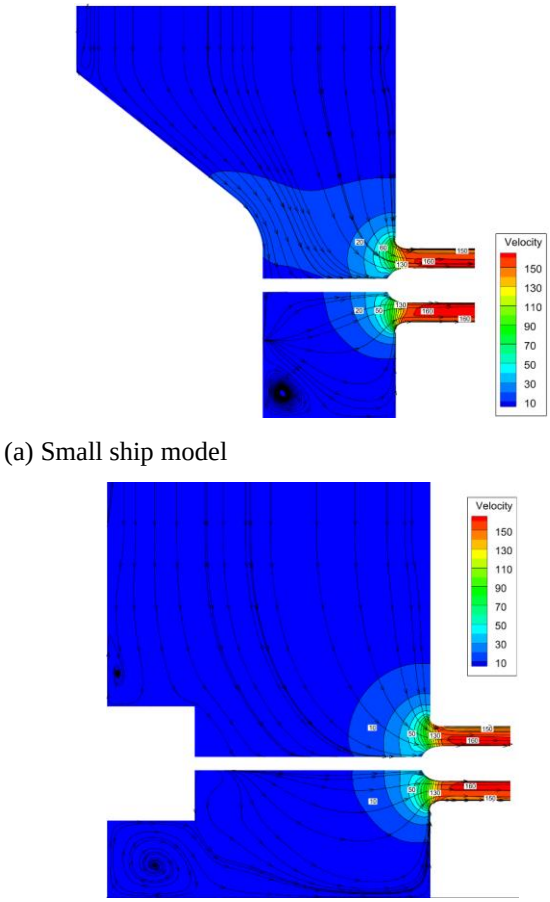

(a) Small ship model

(b) Modified small ship model

Fig. 10 Velocity distribution of small ship intake structure

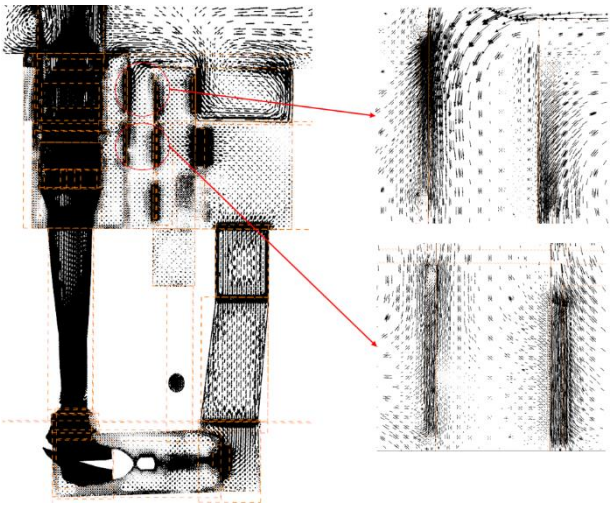

Fig. 11 Schematic diagram of air intake and exhaust systems

behaviour of the intake system was similar after the intake structure was changed, based on the actual situation of the ship.

As shown in Fig. 10, there are two types of velocity distributions for the intake structures of small boats. In Fig. 10(a), the flow cross-section gradually decreases after the airflow enters through a louver, resulting in the airflow being halted by the wall. This created a reflux zone on the left side of the bottom. Because of the compressor suction effect, the air flow exhibited a clear velocity gradient near the fairing and entered the compressor after a 90° flow transition. Owing to the asymmetric design of the inlet structure and impact of the reflux zone, the flow at the inlet section of the compressor was nonuniform. As shown in Fig. 10(b), the reducer installed in the pressure-stabilising chamber significantly enhanced the airflow space. The structure of the pressure-stabilising chamber was predominantly symmetrical. The reflux zone created by the wall was far from the compressor inlet, minimizing its contribution to the uneven flow at the compressor inlet and reducing distortion. The comparison of the velocity cloud charts in Fig. 10 suggests that installing a reducer in the pressure-stabilising chamber can significantly improve the airflow, assuaging the issues of flow asymmetry and distortion at the compressor inlet.

As shown in Fig. 11, there is an air-robbing phenomenon between the exhaust jet and intake shutters, particularly for the shutters located in the upper layer of the exhaust jet. When the gas from the ocean environment

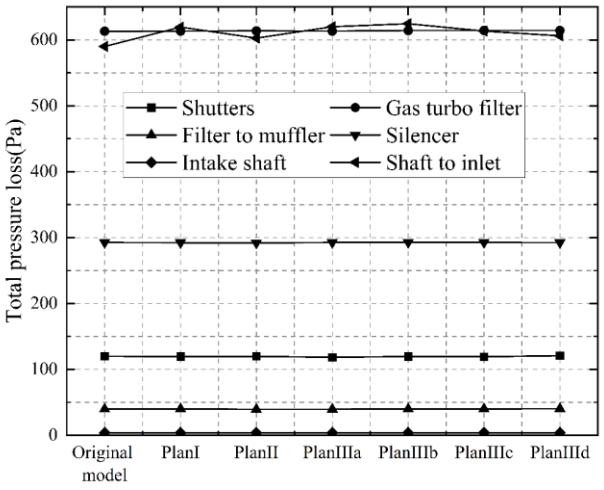

Fig. 12 Total pressure loss of intake components

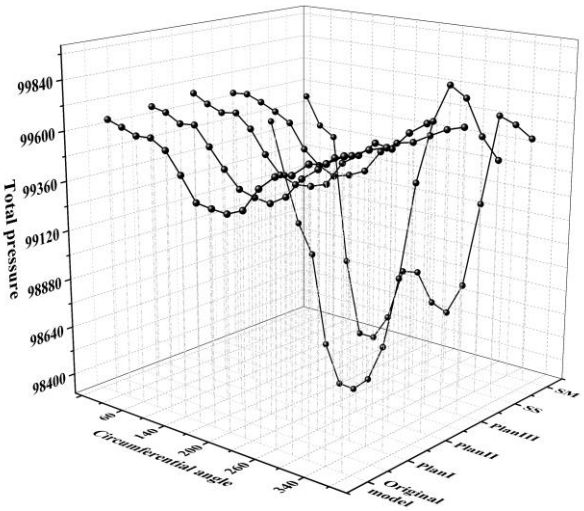

Fig. 13 Total pressure distribution of the compressor inlet section with different intake structures

enters the middle position of the intake and exhaust system shutters, most of it enters the intake system because of the greater negative pressure of the intake shutters. The exhaust jet shutters do not receive sufficient cool air, and this affects the jet ability of the exhaust system. Therefore, the influences of the exhaust system and hull need to be considered when studying the intake system flow of large ships, to improve the accuracy of the research results.

The findings in Fig. 12 indicate that for large ships under the same operating conditions, the behaviour of the various intake structure flows from the shutters to the intake shafts are basically the same, and the total pressure loss of the airflow through the intake components is relatively consistent. However, variations in the total pressure loss arise due to structural design modifications in the segment from the shaft exit to the compressor inlet. Plan I, which reduces the volume of the stabilising chamber, and Plan III, which adds a baffle, hinder the smooth flow of gas and lead to an increase in the total pressure loss. Plan II, which changes the angle of the inlet shaft, leads to an increase in the turning angle of the airflow into the compressor, further augmenting the total pressure loss. The results indicate that changes in the inlet structure result in changes in the flow of some inlet components and total pressure loss; however, this does not significantly affect the flow behaviour of the gas and account for only a small part of the total pressure loss in the inlet system.

Figure 13 shows the circumferential variations in the total pressure at the compressor inlet section for different inlet structures. In larger ships, the airflow undergoes multiple rectifications before entering the compressor, resulting in relatively minor effects from changes in the intake structure. The uneven distribution of the total pressure at the compressor inlet was primarily due to the turning transition of the airflow. The results in Fig. 13 indicate that the circumferential angles of the low-pressure areas at the compressor inlet for different large ship structures were 120°, with a total pressure difference of less than 400 Pa between the high- and low-pressure areas. The circumferential distribution pattern of the total pressure is largely consistent. Hence, a change in the intake structure of a large ship does not significantly alter the overall flow of the intake system. In contrast, small ships have a simpler intake structure, and the structure of the pressure chamber and installation position of the compressor are asymmetric, causing a more pronounced airflow unevenness as it enters the compressor after turning. The circumferential angle of the low-pressure area at the inlet of the small ship compressor was 180°, with a total pressure difference of up to 1600 Pa between the high- and low-pressure areas. By optimising the intake structure of small ships, the airflow space increases, and the structural asymmetry weakens. The circumferential area of the low-pressure region remained largely unchanged, but the total pressure difference in the high- and low-pressure regions decreased, leading to enhanced flow uniformity in the compressor inlet section.

The compressor inlet cross-sectional data of different intake structures were processed, and the unevenness of the compressor inlets of the different intake structures were obtained (Fig. 14).

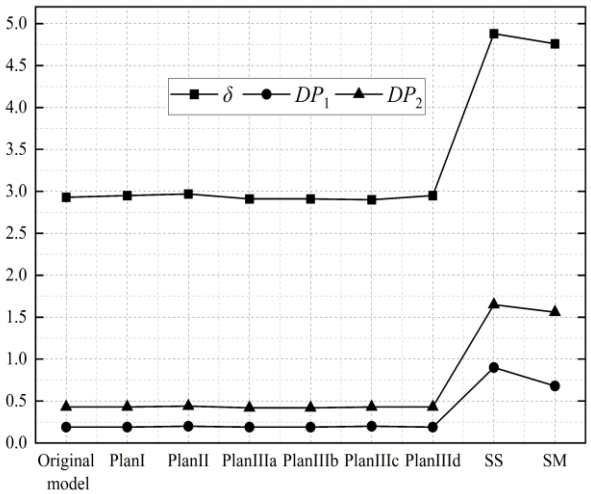

Fig. 14 Nonuniformity of the compressor inlet with different intake structure

The findings presented in Fig.14 illustrate that the inlet structure of the ship significantly impacted the inlet section of the compressor, resulting in velocity and total pressure distortions. The results showed that the variation of inlet structures in large ships caused approximately 3% of the overall distortion in the inlet velocity, whereas the distortion in the total pressure was less than 1% for both types of structures. When the inlet structure was varied within a reasonable range, the velocity and total pressure distortions at the compressor inlet had negligible effect. In contrast, small ship intake systems have a relatively limited intake space and an uncomplicated inlet structure, leading to significant non-uniformity in the flow field at the compressor inlet. As a result, the non-uniformity of the speed can reach up to 5%, whereas the total pressure distortion exceeds 1.5%. In addition, the flow field at the compressor inlet in small-intake systems is significantly more uneven than that in large-gas-turbine intake systems. Different inlet structures in small ships have a noticeable impact on the velocity non-uniformity and total pressure distortion at the compressor inlet. The flow field at the inlet of the modified compressor was more uniform than that at the inlet of the original compressor. This study highlights the importance of an optimised inlet structure design to reduce velocity and total pressure distortions in the compressor inlet section, especially in small marine intake systems.

5. INFLUENCE OF SHIP INLET DISTORTION ON THE COMPRESSOR FLOW

An analysis of the flow in the intake system of the ship showed that the presence of a 90° turning point before the compressor intake inevitably leads to inlet distortion. CFD simulations based on the Stage 35 axial compressor model were conducted to investigate the impact of the distorted inflow of the ship on compressor performance and clearance flow.

A Stage 35 axial compressor was selected as the research object, and its detailed parameters are listed in Table 4.

5.1 Computational Scheme

Stage35 indicates that the transonic axial-flow compressor is a complex rotating machine. The Fluent software is very inclusive but lacks calculation optimisation and post-processing software for rotating machines. To obtain more accurate numerical simulation results, the professional software NUMECA for rotating machinery was selected. Figure 15 presents a comparison

Table 4 Axial compressor parameters

Parameter	Value
Rotor blade number	36
Stator blade number	46
Rotor aspect ratio	1.19
Stator aspect ratio	1.26
Tip clearance, mm	0.408
Test rotating speed, rpm	17188.7
Tip line speed, m/s	454.46

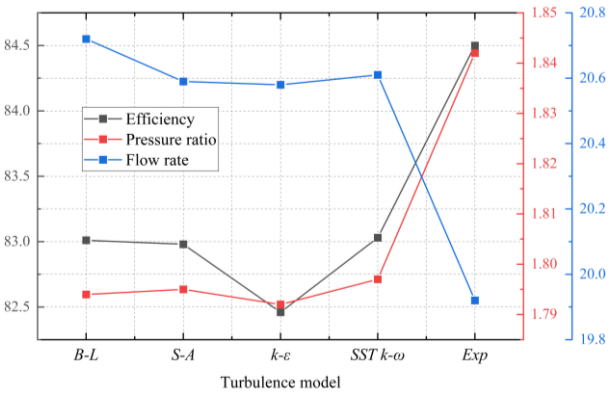

Fig. 15 Turbulence model validation

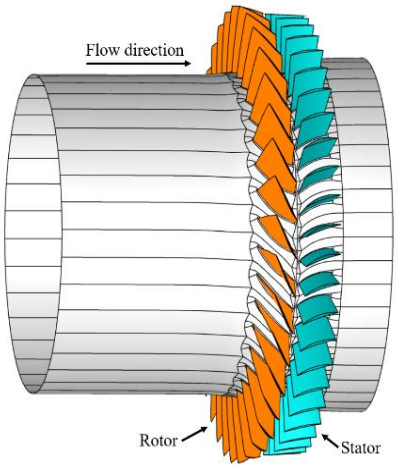

Fig. 16 Axial compressor model simulation area

of the efficiency peak points of the different turbulence models. The S-A turbulence model has a high calculation accuracy, robustness, and a faster rate of convergence. Finally, this turbulence model was selected to solve the Reynolds-averaged Navier–Stokes (RANS) equation, and the convection term was discretised in a high-resolution format. The steady-state calculations were performed using the full-channel grid of the compressor. The inlet boundary was set to the total quantities imposed, with a total inlet temperature of 288.15 K and total pressure of 101325 Pa. The outlet boundary was set to the average static pressure, and the compressor performance curve was obtained by gradually increasing the outlet pressure. In the numerical simulation of the compressor under an inlet distortion, the inlet boundary was changed to the total pressure data of the compressor inlet section obtained in the previous section, and the flow direction was perpendicular to the inlet boundary. Take the last point where parameters such as mass flow rate and efficiency remain stable as the near stall point. The simulation area is shown in Fig. 16.

5.2 Grid Strategy

The computational grids used in this study are illustrated in Fig. 17. The mesh topology for a single passage in each blade row is designated as O-H. The O-meshes are positioned around the blade surfaces, whereas the H-meshes occupy the remaining flow passages. The tip clearance of the rotor was divided by butterfly topology meshes.

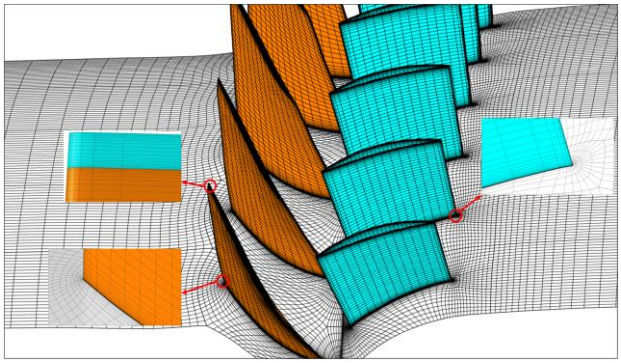

Fig. 17 Computational mesh scheme

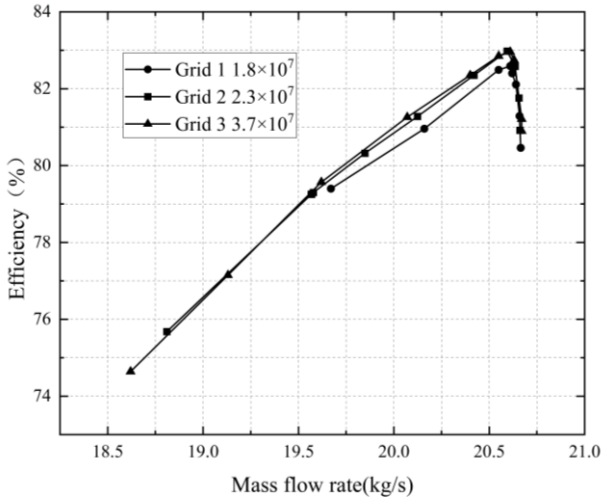

Fig. 18 Grid Scheme Validation

The grid independence was verified using three different grid strategies, as illustrated in Fig. 18. The distance between the first-layer meshes and solid walls was established at a minimum of 1×10^{-5}m. The grid parameters were y^+ <5, minimum orthogonality >15, maximum aspect ratio <1000, and maximum expansion ratio <5. A comparison of the grid-independence results (Fig. 18), indicate that the Grid2 mesh size was adequate to provide a relatively accurate simulation in this case. Therefore, Grid 2 was adopted as the optimal grid in this study.

5.3 Estimate

To verify the feasibility of the numerical simulation method, the obtained numerical simulation results of the operating characteristic curves and flow field parameters of a Stage 35 compressor were compared with that obtained experimentally by Reid and Moore (Fig. 19). As per the graph, the trends of the compressor operating characteristic lines obtained from the numerical simulation and experimental results are identical. However, when the compressor enters the working condition near the stall point, severe separation flow characteristics occur inside. The currently developed turbulence models cannot fully simulate such phenomena, leading to a premature divergence in the numerical calculations. The numerical simulation results of the surge and blockage flow rates were both greater than the experimental values, and the stable operating range obtained via numerical simulation was smaller than the experimental value. Therefore, there is error between the

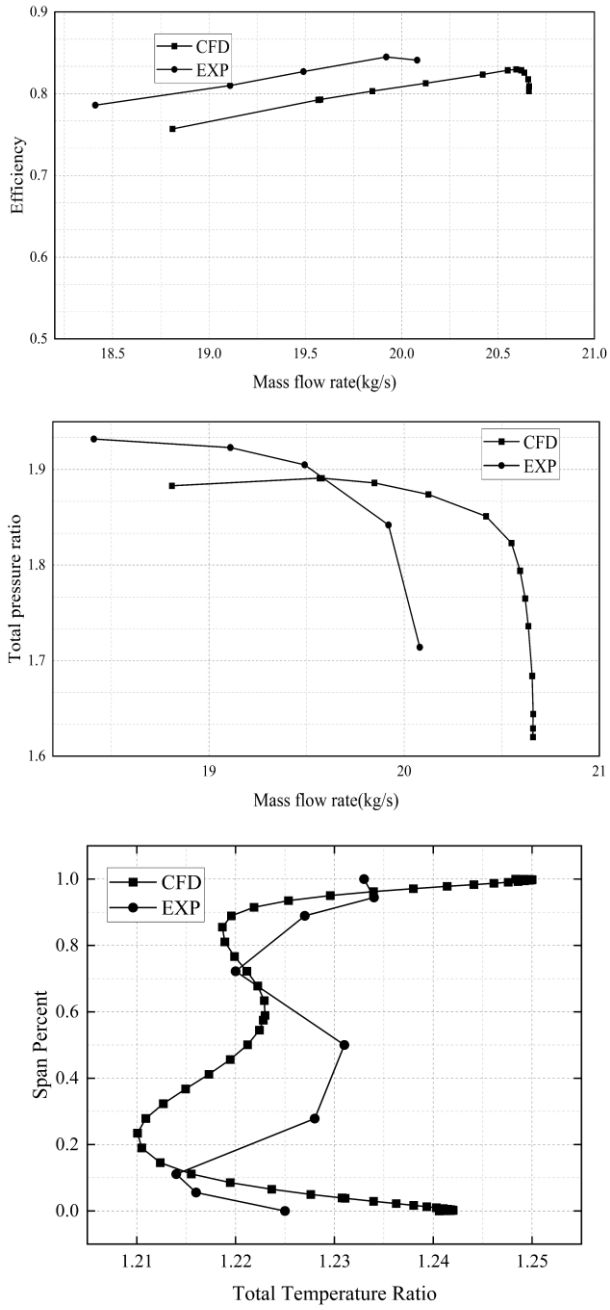

Fig. 19 Comparisons between numerical and experimental results

small operating flow rate of the compressor calculated by the numerical simulation near the stall point and the experimental results. After the turning point at the blade root in the comparison diagram of the total temperature ratio, the total temperature ratio at the radial outlet of the compressor reached its maximum value at a blade height of 0.55 and then, decreased and increased along the blade height. The distribution patterns of the flow parameters obtained from the numerical simulation were consistent with the experimental results. When the operating condition of the compressor is far from the stall point, at the peak efficiency point and an identical flow rate, the errors between the pressure ratio, adiabatic efficiency, and experimental values were within 3%, indicating that the calculation model and numerical simulation method met the accuracy requirements.

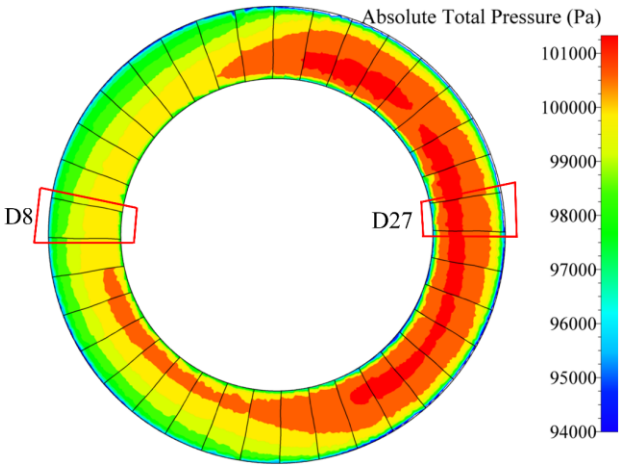

Fig. 20 Ship inlet total pressure distribution with distortion

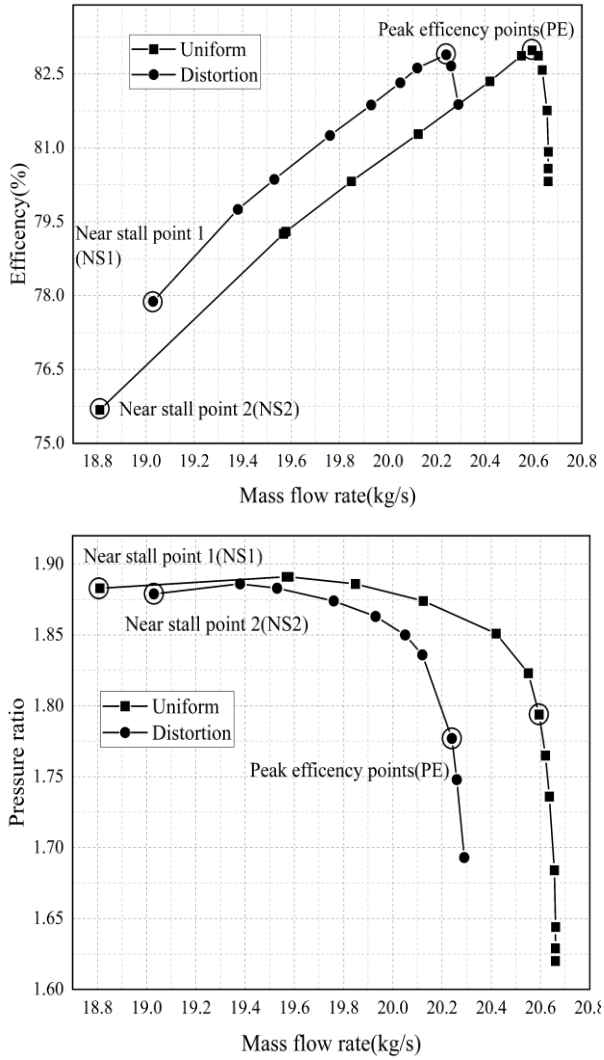

Fig. 21 Comparisons of performance lines under various inlet conditions

5.4 Results (With Inlet Distortion)

Figure 21 shows a comparison of the compressor performance with and without inlet distortion. NS2 is the near-stall operating point of the compressor under distorted conditions, NS1 is the uniform-inflow near-stall operating point, and PE is the highest-efficiency operating point. The total pressure data of the compressor inlet section obtained in the previous section were organised and set as the boundary conditions for the compressor inlet, as shown in Fig. 20. The total pressure change in the mainstream region of the ship inlet distortion, added at the compressor inlet, was less than 3000 Pa. Furthermore, there were circumferential and radial distortions; however, these values were relatively small. The compressor had a strong ability to resist distortion at peak efficiency, resulting in relatively small performance changes due to distortion. Compared with the uniform intake model, the peak efficiency and pressure ratio of the compressor under distorted intake conditions showed relatively small changes of only 0.32 and 0.26%, respectively. However, the working flow range of the compressor was significantly reduced. According to Equations (5) and (6), the stall margin under uniform intake is 14.91%, whereas that under distorted intake conditions is 12.4%, which is a decrease of 2.51%. The working flow margin was reduced by 2.76%.

5.5 Impacts of Distorted Inflows on Flow Field.

The details of the flow characteristics are discussed in the following sections to understand the negative effects of distortions on the compressor performance.

Figure 22 shows the relative Mach number distributions at different blade heights under uniform and distorted inlet conditions at the PE operating point. Under uniform inlet conditions, there was a clear elongated area with a larger Mach number at a certain angle to the blade at the leading edge and front half of the suction force of the moving blade. At the suction surface of the trailing edge of the moving blade, a large wake region with a small Mach number was observed. At the blade root, there was a cluster of parallel Mach number lines which were equal. The equal Mach number lines were observed from approximately 50% of the pressure surface to approximately 80% of the suction surface of the adjacent blades starting from the leading edge of the blade. Furthermore, the shockwave was located at the leading edge of the blade within the blade root channel. At a blade height of 50 %, the equal Mach number line and starting position of the shock wave in the rotor channel move forward to the leading edge of the moving blade. Because of the high airflow velocity at the mid-diameter, separation occurred earlier on the suction surface, and the wake flow area of the moving blade increased. At 95% of the blade height, the airflow on the pressure surface flowed into the suction surface through the blade tip gap, forming a vortex flow that strongly interfered with the flow field in the channel, resulting an increased range of low-pressure areas. The Mach number distribution in the front half of the blade suction was no longer regular. A pressure difference occurs between the different blade channels when there is a total pressure distortion at the compressor inlet, resulting in an uneven distribution of the relative Mach numbers in front of the moving blades. As the flow developed, the influence of the distortion between the blade channels gradually weakened, and the flow state in each channel of the stationary blade became essentially the same.

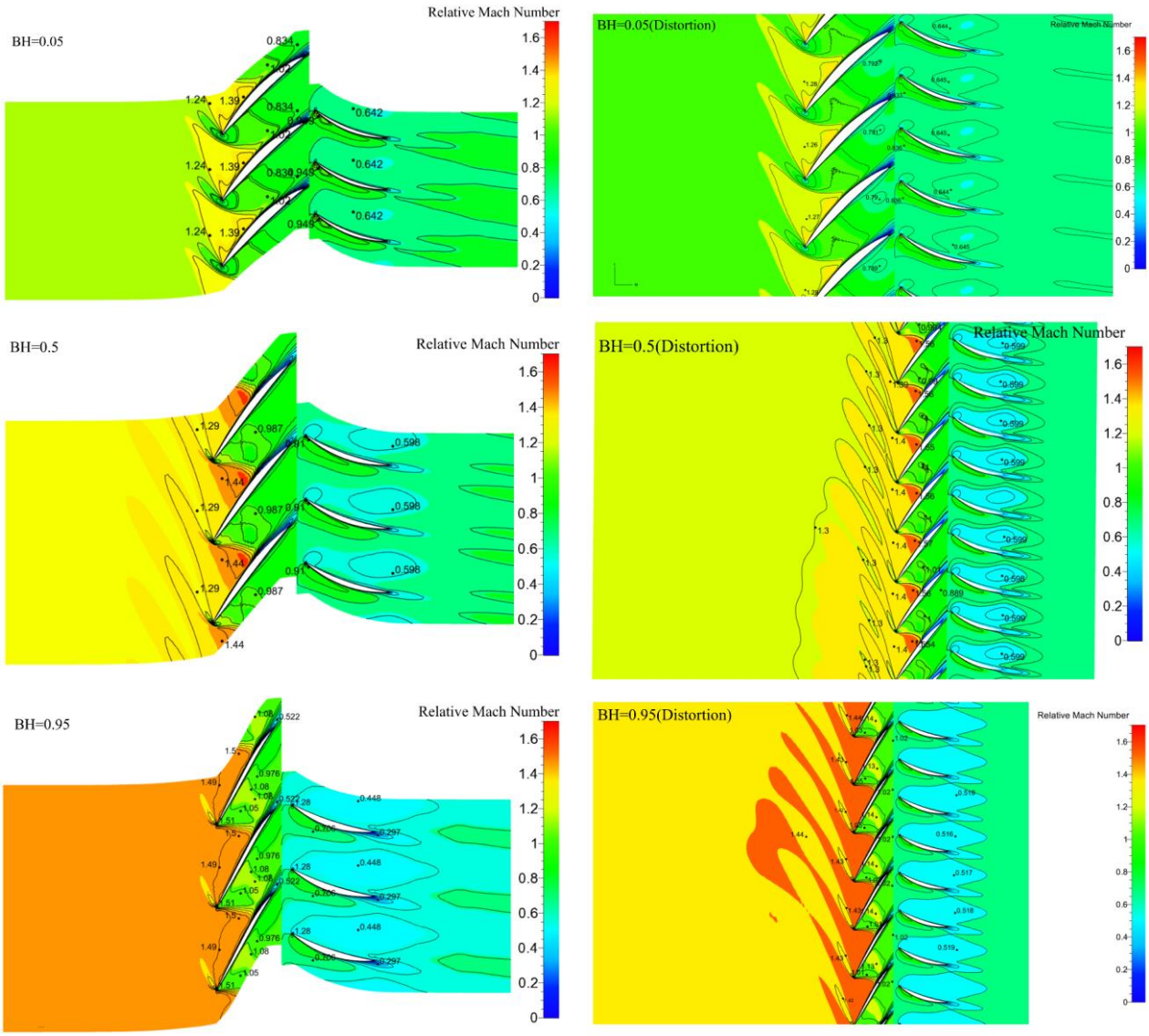

Fig. 22 Relative Mach number distribution at 5, 50, and 95% blade heights under PE conditions

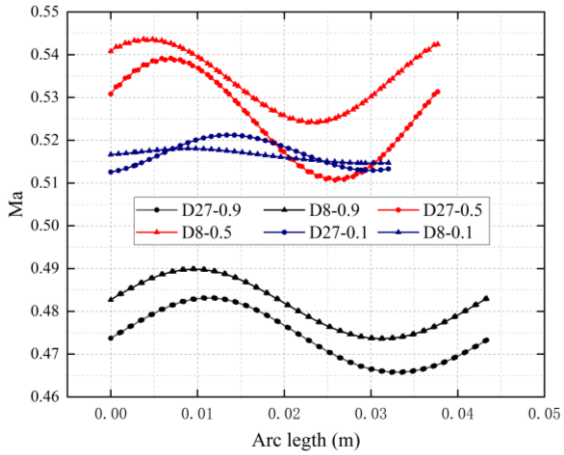

Fig. 23 Ma distribution different blade heights in the D8 and D27 channels for NS2 conditions

Figure 23 shows the distribution of the circumferential Mach number at different blade heights in channels D8 and D27, located before the compressor inlet. The D27 channel experienced an increased pressure gradient in both the circumferential and radial directions compared to the D8 channel, resulting in a greater variation in the circumferential Mach number distribution at different blade heights. At a blade height of 0.1, the flow velocities in both channels were almost identical. However, at blade heights of 0.5° and 0.9°, the distribution pattern of the Mach number remained the same, but there was a notable difference between the flow velocities in the channels. Channels with higher Mach numbers at the compressor inlet were prone to flow separation and tip leakage, resulting in unstable flows.

Figure 24 shows a cloud diagram of the entropy distribution near the stall point under inlet distortion. The figure shows that the boundary layer separation of the moving and stationary blades caused a large flow loss area, whereas the circumferential and radial inlet distortions led to an uneven distribution of pressure and velocity among the rotor blade channels. Additionally, the flow loss in some channels increased significantly. The distortion caused an increase in the gradient of flow changes in some channels, and stalling occurred earlier in such channels as the load increased.

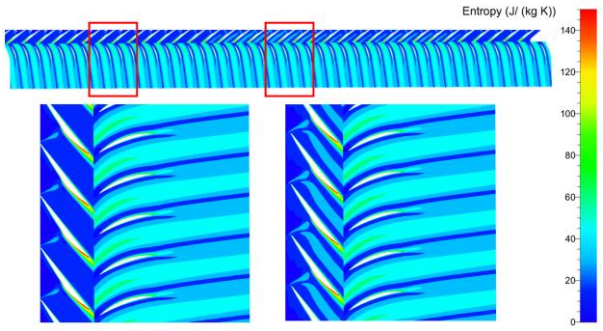

Fig. 24 Entropy distribution under distorted inlet conditions at NS2

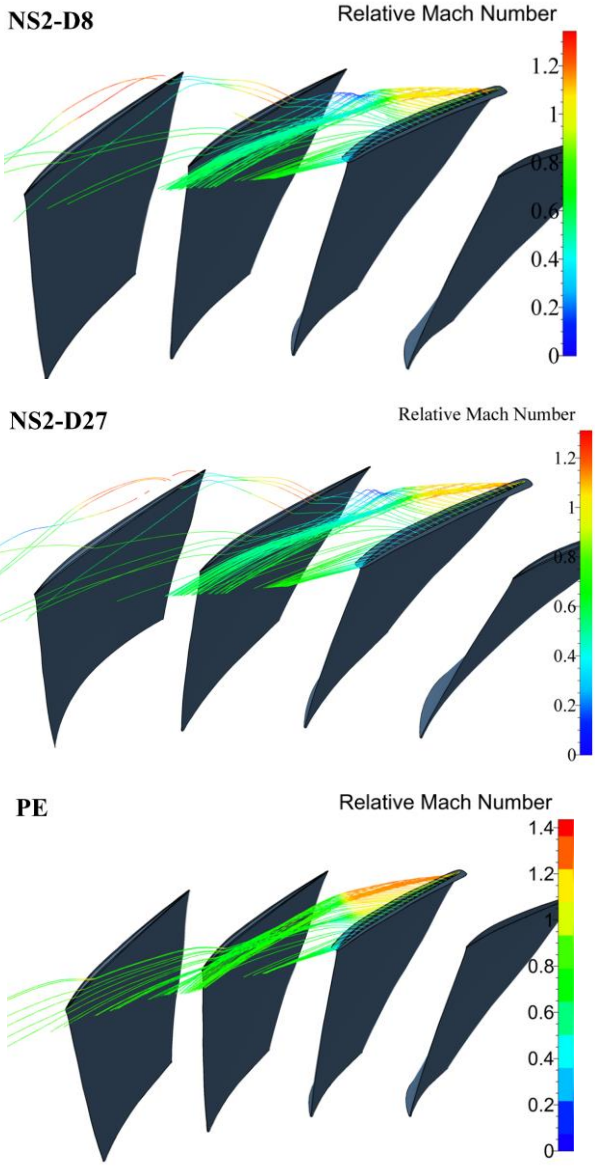

Fig. 25 Leakage flow in the blade tip gap

As shown in Fig. 25, the main leakage flow enters the suction surface through the pressure surface of the leading edge of the driven blade at the tip clearance. It converged with the main flow under the shear effect of the boundary layer on the inner wall of the casing, changed the flow direction to form a vortex, and continued to develop downstream. A small amount of secondary leakage flow flowed through the tip gap of the adjacent blades, resulting in an increased angle between the flow direction and blade body. The secondary leakage flow converged with the main stream in the next channel, near the trailing edge of the blade pressure surface. The leakage flow formed a large range of low-speed vortex flows at the trailing edge of the moving blade pressure surface. The low-energy fluid in the leakage flow was the main reason for the compressor entering a stall state. When the inlet distortion occurred, the distributions of the inlet pressure and flow velocity in each channel differed. The secondary leakage flow at the top of the blade in channel D8 entered the leading edge of the pressure surface of the moving blade in channel D10 at a more forward position, forming stronger vortices in the next channel, and causing the flow in the channel to deteriorate. Stall cells were generated in this channel in advance as the compressor continued to operate and develop into a stall state, resulting in a decrease in the compressor operating margin.

6. CONCLUSION

This article presents a study of marine gas turbine intake, exhaust systems, and compressors via numerical simulation. This study investigated the influence of the intake system structure on the flow field of the intake system, as well as the performance and flow field changes of the compressor under ship distortion. The main conclusions of this study are as follows.

1. A simulation of the intake systems of large ships revealed an air-grabbing phenomenon between the intake and exhaust systems. The exhaust system can affect the flow field of the intake system. Hence, conducting an overall simulation of the intake, exhaust systems, and hull is crucial.

2. This study investigated the influence of the ship intake structure on the compressor intake section, which causes velocity and total pressure distortion. The influence of the different intake structures on the velocity and total pressure distortion is minimal because of the rectification effects of the flow components and pipelines in the intake systems of large ships. However, the intake structure of small ships is relatively simple. Hence, the distortion of the compressor inlet flow field is significantly greater than that of large ships. The modification of the intake structure can effectively increase the stability of the flow field.

3. The study found that an uneven flow velocity and pressure distribution in the upstream compressor inlet after inlet distortion can cause leakage flows from some channels to overflow to the adjacent blade channels at the leading edge of the higher blade span. This overflow causes the compressor entering a stall state, thereby reducing the operating margin.

Overall, this study provides valuable insights into the influence of intake system structure on the flow field of marine gas turbine intake systems and compressors. These findings provide significant insights for the development of efficient and stable intake and exhaust systems for gas turbines.

ACKNOWLEDGEMENTS

The work of this paper was completed with the support of the Research on Equivalent Simulation Test Technology of Total Pressure Distortion (2017-V-0002-0051), and I would like to express my sincere gratitude.

CONFLICT OF INTEREST

Z. Y. Wang, **C. X. He**, and **Y. L. Qu**, declare that they have no conflict of interest.

AUTHORS CONTRIBUTION

Z. Y. Wang designed the research. **Y. L. Qu** provided financial support and experimental resources. **Y. L. Qu** and **C. X. He** conducted research experiments and data processing. **C. X. He** wrote the first draft of the manuscript. **Z. Y. Wang** helped to organize the manuscript and guided the entire research guidance for the entire research.

REFERENCES

Bricknell, D. J. (2006). *Marine gas turbine propulsion system applications.* ASME GT. https://doi.org/10.1115/GT2006-90751

Charalambous, N., Ghisu, T., Iurisci, G., Pachidis, V., & Pilidis, P. (2004). *Axial compressor response to inlet flow distortions by a CFD analysis.* ASME Paper. https://doi.org/10.1115/GT2004-53846

Chen, C., Guan, G., & Sun, Y. (2016). Numerical simulation of the aerodynamic performance of marine gas turbine intake system. *Marine Technology, (5)*, 76-81. https://doi.org/10.3969/j.issn.1000-3878.2016.05.016

Cossar, B. F. J., Moffatt, W. C., & Peacock, R. E. (1980). Compressor rotating stall in uniform and nonuniform flow. *ASME Journal of Engineering Gas Turbines Power*, *102*(4), 762–769. https://doi.org/10.1115/1.3230338

Dong, X., Sun, D., Li, F., Jin, D., Gui, X., & Sun, X. (2018). Effects of stall precursor-suppressed casing treatment on a low-speed compressor with swirl distortion, *ASME Journal of Fluids Engineering Transactions* *140*(9), 091101. https://doi.org/10.1115/1.4039707

Fidalgo, V. J., Hall, C. A., & Colin, Y. (2012). A study of fan-distortion interaction within the NASA rotor 67 transonic stage, *ASME Journal of Turbomachinery* *134*(5), 051011. https://doi.org/10.1115/1.4003850

Fuqun, C., Wenlan, L., Zongyuan, W., & Mengzi, C. (1985). *An experimental investigation of response of a turbojet engine to inlet distortion.* ASME Paper. https://doi.org/10.1115/85-IGT-12

Hah, C., Rabe, D. C., Sullivan, T. J., & Wadia, A. R. (1996). *Effects of inlet distortion on the flow field in a transonic compressor rotor*. ASME Paper. https://doi.org/10.1115/1.2841398

Hirai, K., Kodama, H., Nozaki, O., Kikuchi, K., Tamura, A., & Matsuo, Y. (1997). *Unsteady three-dimensional analysis of inlet distortion in turbomachinery*. AIAA. https://doi.org/10.2514/6.1997-2735

Hynes, T. P., & Greitzer, E. M. (1987). A method for assessing effects of circumferential flow distortion on compressor stability, *ASME Journal of Turbomachinery* *109*(3), 371–379. https://doi.org/10.1115/1.3262116

Jahani, Z., Khaleghi, H., & Tabejamaat, S. (2022). Using tip injection to stability enhancement of a transonic centrifugal impeller with inlet distortion. *Journal of Applied Fluid Mechanics*, *15*(6), 1815-1824. https://doi.org/10.47176/jafm.15.06.1089

Li, J., Du, J., Liu, Y., Zhang, H., & Nie, C. (2020). Effect of inlet radial distortion on aerodynamic stability in a multi-stage axial flow compressor. *Aerospace Science and Technology*, *105*, 105886. https://doi.org/10.1016/j.ast.2020.105886

Shi, B., Sun, H., Liu, S., & Zhang, Y. (2004). The application of les in the study of inlet flow field in marine gas turbine. *Turbine Technology*, 269-271. https://doi.org/10.3969/j.issn.1001-5884.2004.04.010

Soemarwoto, B. I., Boelens, O. J., & Kanakis, T. (2016). Aerodynamic design of gas turbine engine intake duct. *Aircraft Engineering and Aerospace Technology*. https://doi.org/10.1108/aeat-02-2015-0063

Sun, D., Li, J., Dong, X., Gu, B., & Sun, X. (2018). *Effects of rotating inlet distortion on two-stage compressor stability with stall precursor-suppressed casing treatment*. ASME Paper. https://doi.org/10.1115/GT2018-76701

Sutherland, K. (2008). Air filtration in industry: Gas turbine intake air filtration. *Filtration and Separation*, *45*, 20-23. https://doi.org/10.1016/S0015-1882(08)70025-9

Wang, J., Wu, W., Zhong, J., & Pan, T. (2017). Aerodynamic characteristics of the intake system in a marine gas turbine. *Journal of Dalian Maritime University*, *43*, 33-39. https://doi.org/10.16411/j.cnki.issn1006-7736.2017.01.006

Wen, X., & Xiao, M. (2010). Analysis of modern marine gas turbine development tendency. *Ship Science and Technology*, *32*, 3-6. https://doi.org/10.3404/j.issn.1672-7649.2010.08.001

Winter, M. (2009). Systems and methods for altering inlet airflow of gas turbine engines. *Patent, US20090092482A1*. https://patentimages.storage.googleapis.com/99/0d/c6/86695ae37f33c1/US9169779.pdf

Xu, X., Liu, C., Sun, Y., & Zhang, Y. (2014). Numerical simulation on interior flow field for a gas turbine inlet system. *Aeroengine*, *40*, 51-55. https://doi.org/10.13477/j.cnki.aeroengine.2014.02.010

Yao, J., Gorrell, S. E., & Wadia, A. R. (2010). High-fidelity numerical analysis of per-rev-type inlet distortion transfer in multistage fans—part I: Simulations with selected blade rows. *ASME Journal of Turbomachinery 132*(4), 041014. https://doi.org/10.1115/1.3148478

Zhang, M., & Zheng, X. (2018). Criteria for the matching of inlet and outlet distortions in centrifugal compressors. *Applied Thermal Engineering, 131*, 933–946. https://doi.org/10.1016/j.applthermaleng.2017.11.140.

Zhao, B., Sun, H., Wang, L., & Song, M. (2017). Impact of inlet distortion on turbocharger compressor stage performance. *Applied Thermal Engineering, 124*, 393–402. https://doi.org/10.1016/j.applthermaleng.2017.05.181